Hindawi Publishing Corporation
Mathematical Problems in Engineering
Volume 2012, Article ID 546364, 18 pages
doi:10.1155/2012/546364

Research Article

Chaos in a Magnetic Pendulum Subjected to Tilted Excitation and Parametric Damping

C. A. Kitio Kwuimy,[1] C. Nataraj,[1] and M. Belhaq[2]

[1] *Center for Nonlinear Dynamics and Control, Department of Mechanical Engineering, Villanova University, 800 Lancaster Avenue, Villanova, PA 19085, USA*
[2] *Laboratory of Mechanics, University Hassan II, Casablanca, Morocco*

Correspondence should be addressed to C. A. Kitio Kwuimy, cedrick.kwuimy@villanova.edu

Received 18 May 2012; Revised 3 August 2012; Accepted 3 August 2012

Academic Editor: Stefano Lenci

Copyright © 2012 C. A. Kitio Kwuimy et al. This is an open access article distributed under the Creative Commons Attribution License, which permits unrestricted use, distribution, and reproduction in any medium, provided the original work is properly cited.

The effect of tilted harmonic excitation and parametric damping on the chaotic dynamics in an asymmetric magnetic pendulum is investigated in this paper. The Melnikov method is used to derive a criterion for transition to nonperiodic motion in terms of the Gauss hypergeometric function. The regular and fractal shapes of the basin of attraction are used to validate the Melnikov predictions. In the absence of parametric damping, the results show that an increase of the tilt angle of the excitation causes the lower bound for chaotic domain to increase and produces a singularity at the vertical position of the excitation. It is also shown that the presence of parametric damping without a periodic fluctuation can enhance or suppress chaos while a parametric damping with a periodic fluctuation can increase the region of regular motions significantly.

1. Introduction

Various nonlinear phenomena have been found in physical systems and chaotic behavior has been reported in various engineering systems with applications in microelectromechanical [1–3], electromechanical [4–6], mechanical [7–10], electronic [11–13], and others. Usually, numerical indicators such as the Lyapunov exponent and bifurcation diagram are used to determine and study the occurrence of chaos. The Melnikov method [14], on the other hand, predicts analytically the lower bound in parameter space separating regular and chaotic dynamics. The Melnikov method has been recently applied in experimental and theoretical research in various fields of science, including epidemiology [15], biology [16], and engineering systems [2, 7, 8]. Along these lines, Cicogna and Papoff [17] considered a Duffing type potential with an additional linear term and estimated the threshold condition for the appearance of chaos by using a Taylor expansion with respect to the asymmetric

parameter. The optimal control of chaos was studied by Lenci and Rega [18] for the Helmholtz-Duffing oscillator. Litak et al. [19] revisited the Melnikov criteria for a driven system under a single and double well asymmetric potential and expressed the integrals to be evaluated for the appearance of chaos in terms of logarithm function. Cao et al. [20] applied the Melnikov theory to a driven Helmholtz-Duffing oscillator and derived the condition for appearance of fractal basin boundaries. Recently, a magnetic pendulum driven by a high-frequency excitation under a magnetic potential was considered [21]. This paper aims to apply the well-known Melnikov theory to a fundamental physical device used in several engineering systems, namely, a magnetic pendulum, and discuss the possibility of chaos suppression in the system.

Current literature examines various nontrivial phenomena caused by a high-frequency excitation in physical systems. Thomsen [22] considered the stiffening, biasing, and smoothening in such systems, Bartuccelli et al. [23] and Schmitt and Bayly [24] showed that a high-frequency excitation of a horizontally or vertically shaken pendulum results in oscillations about a nonzero mean angle. Yabuno et al. [25] considered an inverted pendulum and showed that a tilt angle of the excitation produces stable equilibrium states different from the direction of the gravity and the excitation. The symmetry breaking bifurcation due to the tilt angle was also investigated qualitatively and through experiments by Mann and Koplow [26]. In a related experimental work, Mann investigated the energy criterion for snap-through instability and nonperiodic motion.

The effect of a fast parametric excitation on self-excited vibrations in a delayed van der Pol oscillator was reported in [27, 28]. Fidlen and Juel Thomsen [29] analyzed this effect on the equilibrium of a strongly damped system comparing to the case of a slightly damped one. Mann and Koplow [26] showed that a small deviation from either a perfectly vertical or horizontal excitation will result in symmetry breaking bifurcations opposed to pitchfork bifurcations obtained for vertical or horizontal excitation. Also, the condition for well escapes in a bistable configuration of the potential energy has been studied [21]. An earlier work on magnetic pendulum was done by Moon et al. [30] who showed evidence of homoclinic orbit and horseshoe chaos in a magnetic pendulum. Kraftmakher [31] reported that parametric damping has some strong effects on the stabilization dynamics of a pendulum. The effects of the sinusoidal fluctuation arising from a control strategy was also considered. Recently, Sah and Belhaq [32] investigated the tilting effect of a fast excitation on self-excited vibrations in a delayed van der Pol pendulum.

It thus appears from this paper that, parametrically excited magnetic pendulum is an interesting system from both the mathematical and physical points of view. The present work was motivated by the experimental work carried out by Mann [21] in which the basins of attraction have been computed and the influence of parametric excitation on escape phenomena have been studied. Specifically, we consider the experimental system as in [21] and we investigate analytically and numerically the tilting effect of the parametric excitation as well as the time-dependent parametric damping on the basins of attraction and on chaos domain in the parameter space of the system. In other words, the present paper can be considered as an extension of the experimental work [21] in adding other effects to the original system.

To identify the conditions leading to nonperiodic response, Melnikov method is applied using the Gauss hypergeometric function. The use of this function can be considered as an extension of the work by Litak et al. [19]. To the best of our knowledge, the effect of tilted excitation and parametric damping on the appearance of chaos in magnetic pendulum

has not been addressed. In addition to being of fundamental interest, this paper expects to impact practical design and control of systems involving a magnetic pendulum.

The paper is organized as follows. In Section 2, the mathematical model and the corresponding homoclinic orbit are given. In Section 3, the Melnikov theorem is used to obtain the threshold condition for the appearance of chaos and the basins of attraction are explored to support the Melnikov results. Attention is focused on the effects of the titling of the excitation on the chaos occurrence, in the absence of parametric damping. In Section 4, parametric damping is introduced and its effect is analyzed. Section 5 concludes the work.

2. The Model and Hamiltonian System

A schematic representation of the pendulum is shown in Figure 1 where θ is the angular deviation, m and L are the mass and the effective length of the pendulum, respectively, A and Ω are the amplitude and the frequency of the excitation, respectively, and γ is the tilt angle of the excitation with respect to the gravity direction. Using Newton's laws it is shown that the mathematical model describing the angular oscillations of the system can be written as [21, 26]

$$\frac{d^2\theta}{d\tau^2} + \frac{c}{mL^2}\frac{d\theta}{d\tau} + \frac{g}{L}\sin\theta + \frac{1}{mL^2}\frac{\partial U}{\partial\theta} = \frac{A\Omega^2}{L}\cos\Omega\tau\cos(\theta-\gamma), \tag{2.1}$$

where θ is the angular deviation, τ is the time, c is the damping coefficient, m and L are the mass and the effective length of the pendulum, respectively, g is the acceleration due to gravity, A and Ω are the amplitude and the frequency of excitation, respectively, γ is the tilt angle of the excitation with respect to the horizontal direction, and $U(\theta)$ is a nonsymmetric potential defining the nonlinear restoring force of the magnet given as [21]

$$U(\theta) = \frac{a_1}{2}\theta^2 + \frac{a_2}{3}\theta^3 + \frac{a_3}{4}\theta^4 + \text{high order terms}, \tag{2.2}$$

where a_1, a_2, and a_3 are physical constants. By expanding $\cos\theta$ and $\sin\theta$ up to the third order, (2.1) becomes in dimensionless form

$$\frac{d^2x}{dt^2} + \lambda\frac{dx}{dt} + \eta x + \alpha x^2 + \beta x^3 = f(t), \tag{2.3}$$

with

$$\begin{gathered}
f(t) = r\omega^2\left[\zeta_0 + \zeta_1 x + \zeta_2 x^2 + \zeta_3 x^3\right]\cos\omega t, \\
x = \frac{\theta}{\theta_0}, \qquad t = \frac{\tau}{T}, \qquad \lambda = \frac{cT}{2mL^2}, \qquad \eta = \left[\frac{g}{L} + \frac{a_1}{mL^2}\right]T^2, \qquad \alpha = \frac{a_2T^2\theta_0}{mL^2}, \\
r = \frac{A}{2L^2\theta_0}, \qquad \gamma = \frac{\omega^2 A}{2L^2}, \qquad \zeta_0 = \cos\gamma, \qquad \zeta_1 = \theta_0\sin\gamma, \qquad \zeta_2 = -\frac{\theta_0^2}{2}\cos\gamma, \\
\beta = \left[-\frac{g}{6L} + \frac{a_3}{mL^2}\right]T^2\theta_0^2\zeta_3 = -\frac{\theta_0^3}{6}\sin\gamma, \qquad \omega = \Omega T,
\end{gathered} \tag{2.4}$$

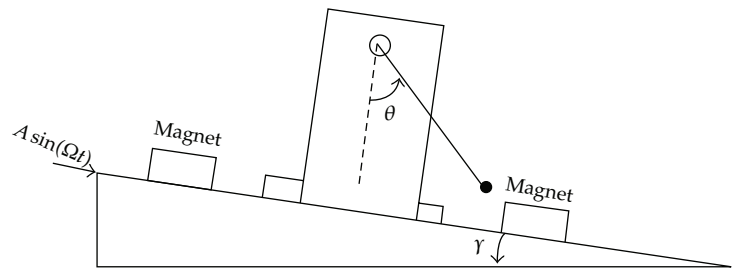

Figure 1: Schematic representation of the pendulum.

where θ_0 and T are, respectively, the characteristic angle and the time used to rescale the modeling equation. It is important to note that the case $\gamma = 0$ corresponds to the horizontal excitation ($\zeta_1 = 0$), while the case $\gamma = \pi/2$ corresponds to the vertical excitation ($\zeta_0 = 0$). The signs of η, α, and β change with the characteristic of the magnetic potential; see for instance the experiment carried out in [21] in which $\eta < 0$, $\alpha > 0$, and $\beta > 0$. In order to perform a general analysis, the dimensionless parameters are used and their values are meaningfully selected according to the available literature. Without loss of generality, we choose in the rest of the paper $\eta < 0$, $\alpha > 0$, and $\beta > 0$. The following Hamiltonian system, obtained from (2.3)

$$\frac{dx}{dt} = y, \qquad \frac{dy}{dt} = -\eta x - \alpha x^2 - \beta x^3 \tag{2.5}$$

leads to the Hamiltonian function

$$\mathbf{H}(x, y) = \frac{1}{2}y^2 + \frac{dV(x)}{dx}, \tag{2.6}$$

where $V(x)$ is given by following asymmetric potential

$$V(x) = \frac{1}{2}\eta x^2 + \frac{1}{3}\alpha x^3 + \frac{1}{4}\beta x^4. \tag{2.7}$$

This potential has two stable and one unstable equilibrium points given by $x_s^{l,r} = (-\alpha \pm \sqrt{\alpha^2 - 4\eta\beta})/2\beta$ and $x_{\text{un}} = 0$, where the letters l and r stand for the left and right hand side, respectively. It is obvious that $V(x_{\text{un}}) = 0$ and by comparing $V(x_s^l)$ and $V(x_s^l)$, one concludes that the left well is always deeper if $\eta < 0$ and it is deeper for $\eta > 0$ if $\alpha < 2\sqrt{\eta\beta}$. The Hamiltonian defined in (2.6) has an hyperbolic fixed point at $x = 0$ and two elliptic fixed points at $x_{l,r} = (-2\alpha \pm \sqrt{4\alpha^2 - 18\eta\beta})/3\alpha$ leading to the homoclinic orbit given by

$$\begin{aligned} x^{l,r} &= \frac{-2\eta}{2\alpha/3 \pm \sqrt{\Delta}\cosh\sqrt{-\eta}t}, \\ y^{l,r} &= \frac{\pm 2\eta\sqrt{-\eta\Delta}\sinh\sqrt{-\eta}t}{\left[2\alpha/3 \pm \sqrt{\Delta}\cosh\sqrt{-\eta}t\right]^2}, \end{aligned} \tag{2.8}$$

with $\Delta = 4\alpha^2/9 - 2\eta\beta$.

Figure 2(a) shows asymmetric potentials and orbits with different depths for the left and right wells. The shape of the orbits on the left and right sides of the saddle point is different as shown in Figure 2(b). As the asymmetric term increases, the deepness of the left well becomes large compared to the right one. In order to analyze the condition for the appearance of chaos in the magnetic pendulum with a tilted excitation, we apply the Melnikov method.

3. Melnikov Analysis and Basin of Attraction

In order to perform the Melnikov analysis, the perturbed Hamiltonian equation (2.5) is rewritten as

$$\frac{d}{dt}\begin{pmatrix} x \\ y \end{pmatrix} = \mathbf{F}(x,y) + \epsilon \mathbf{G}(x,y,t-t_0), \tag{3.1}$$

where

$$\mathbf{F}(x,y) = \begin{pmatrix} y \\ -\eta x - \alpha x^2 - \beta x^3 \end{pmatrix},$$
$$\mathbf{G}(x,y,t-t_0) = \begin{pmatrix} 0 \\ -\lambda^* y + r^* \omega^2 \left[\sum_{i=0}^{i=3} \zeta_i x^i\right] \cos\omega(t-t_0) \end{pmatrix}, \tag{3.2}$$

where t_0 being a phase angle, ϵ is a perturbation parameter, $r = \epsilon r^*$, and $\lambda = \epsilon\lambda^*$. In the rest of the paper, the stars are removed for simplicity. For $\epsilon = 0$, the homoclinic orbit connects the unstable point x_{un} and the eigenvalues of the linearized problem around x_{nu} are real and of opposite sign. For $\epsilon \neq 0$, the Melnikov theorem can be used to detect transverse intersections between perturbed stable and unstable manifolds in the system. According to [14], the distance between the perturbed and unperturbed manifolds is given by the Melnikov function:

$$M(t_0) = \int_{-\infty}^{+\infty} \mathbf{F}(x,y) \times \mathbf{G}(x,y,t-t_0)\,dt, \tag{3.3}$$

which can be written as

$$M(t_0) = -\lambda J_0 + r\omega^2 \left[\sum_{i=0}^{i=3} \zeta_i I_i\right] \sin\omega_0 + r\omega^2 \left[\sum_{i=0}^{i=3} \zeta_i I_{i+4}\right] \cos\omega t_0. \tag{3.4}$$

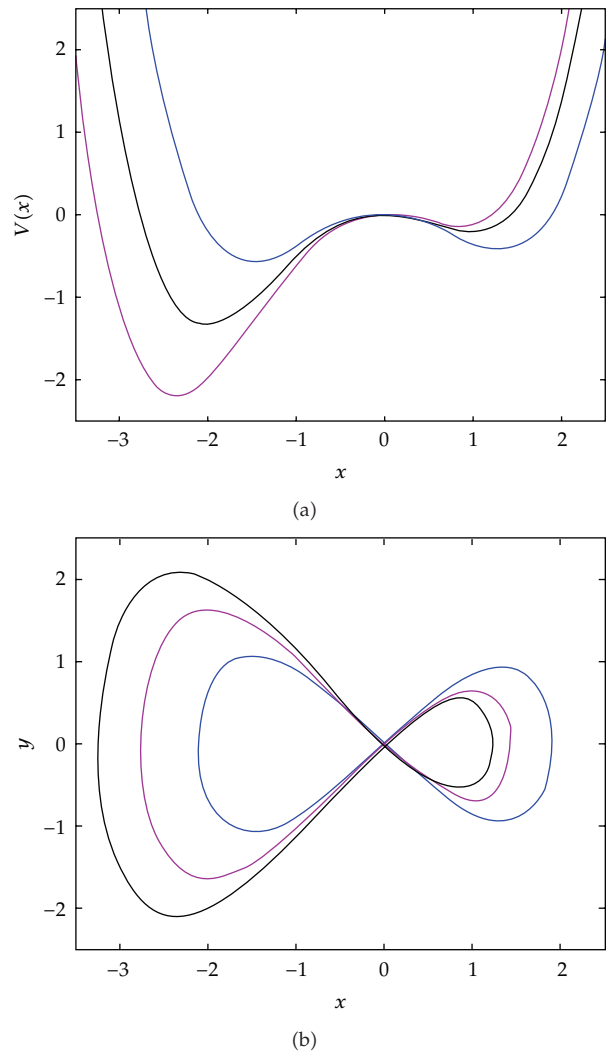

Figure 2: Asymmetric potential and separatrix showing the depth and shape difference between the left and right side. (a) Asymmetric potential. (b) Asymmetric separatrix. $\eta = -1$, $\beta = 0.5$, and $\alpha = 0.075$: blue line, $\alpha = 0.5$: black line, and $\alpha = 0.75$: magenta line.

The integrals $J_0^{l,r}$ and $I_i^{l,r}$, $i = 0, \ldots, 7$ are evaluated hereafter. For the integral $J_0^{l,r}$ we have

$$\begin{aligned} J_0^{l,r} &= \int_{-\infty}^{+\infty} y_0^{l,r\,2}\, dt = \int_{-\infty}^{+\infty} \frac{-4\eta^3 \Delta \sinh^2 \sqrt{-\eta}t}{\left[2\alpha/3 \pm \sqrt{\Delta}\cosh\sqrt{-\eta}t\right]^4} dt \\ &= \frac{-81\eta^2\Delta\sqrt{-\eta}}{\alpha^4} \frac{\Gamma(2)\Gamma(3/2)}{\sqrt{\pi}\Gamma(4)} \frac{\mu^4}{\sqrt{\mu^2-1}} \mathbf{Q}_2^1(\mu), \end{aligned} \tag{3.5}$$

where μ is defined for the left and the right side such that $\sqrt{\mu^2-1}/\mu = \pm 3\sqrt{\Delta}/2\alpha$, $\mathbf{\Gamma}(z)$ is the Gamma function and $\mathbf{Q}_m^n(z)$ is the associated Legendre function of the second kind. Using the definition, the functional relation of the Gamma function and the associated Legendre function of the second kind (listed in Appendices A and B), the integral $J_0^{l,r}$ becomes

$$J_0^{l,r} = \frac{\eta^2\sqrt{-\eta}}{15\Delta}\,{}_2\mathbf{F}_1\left(1,2;\frac{7}{2};\xi\right), \tag{3.6}$$

where $\xi = 9\eta\beta/(9\eta\beta - 2\alpha^2)$, $J^2 = -1$, and ${}_2\mathbf{F}_1(a,b,c,z)$ is the hypergeometric function. Unfortunately, further simplification of the hypergeometric function can be made only for some specific values of the argument, see [33] for details. Note that in the absence of the magnetic potential ($\alpha = 0$, $\xi = 1$), the device is under a symmetric Duffing potential and then the integral becomes [2, 8, 19]

$$J_0^{l,r} = \frac{4(-\eta)^{3/2}}{3\beta}. \tag{3.7}$$

The Gauss hypergeometric function, for complex or real argument, can be evaluated using the Gnu Scientific Library (GSL) via a PYGSL code [34]. In order to evaluate the other integrals, we define the following functions:

$$\begin{aligned}
\mathbf{K}_1(n,1,\omega) &= \int_{-\infty}^{+\infty} {x_0^{l,r}}^n y_0^{l,r}\sin\omega t\,dt = 2\zeta_0^n\zeta_1\int_0^{+\infty}\frac{\sinh\sqrt{-\eta}t\sin\omega t}{\left[2\alpha/3\pm\sqrt{\Delta}\cosh\sqrt{-\eta}t\right]^{n+2}}dt,\\
&= 2\zeta_0^n\zeta_1\exp(a\pi)\frac{a\nu^{n+2}}{(n+1)\sqrt{\nu^2-1}}\frac{\mathbf{\Gamma}(1+n-Ja)}{\mathbf{\Gamma}(n+1)}\mathbf{Q}_n^{Ja}(\nu),\\
&= \frac{(-1)^n 2^{n+1}\eta\omega\mathbf{\Gamma}(1+n-Ja)\mathbf{\Gamma}(1+n+Ja)}{\Delta^{(n+1)/2}(n+1)n!(2n+1)!}\times{}_2\mathbf{F}_1\left(\frac{n+1-Ja}{2},\frac{n+1+Ja}{2};\frac{2n+3}{2};\xi\right),
\end{aligned} \tag{3.8}$$

with $\zeta_0 = -6\eta/2\alpha$, $\zeta_1 = \pm 9\eta\sqrt{-\eta\Delta}/2\alpha^2$, and $a = \omega/\sqrt{-\eta}$. It can be shown (see Appendix C) that ${}_2\mathbf{F}_1(a,\overline{a},c,z)$ $(a\in\mathbf{C},\ c\in\mathbf{R}_+^*,\ z\in]0,1[)$ is always a positive real number.

$$\mathbf{K}_2(n,1,\omega) = \int_{-\infty}^{+\infty} {x_0^{l,r}}^n y_0^{l,r}\cos\omega t\,dt = 0 \tag{3.9}$$

is considered as a product of odd and even function.

Thus, one has, for the integral $I_0^{l,r}$,

$$\begin{aligned}
I_0^{l,r} &= \int_{-\infty}^{+\infty} y_0^{l,r}\sin\omega t\,dt = \mathbf{K}_1(0,1,\omega)\\
&= \pm\frac{4\pi\omega^2}{\Delta\sinh\left(\omega\pi/\sqrt{-\eta}\right)}\,{}_2\mathbf{F}_1\left(\frac{1}{2}-J\frac{\omega}{2\sqrt{-\eta}},\frac{1}{2}+J\frac{\omega}{2\sqrt{-\eta}};\frac{3}{2};\xi\right),
\end{aligned} \tag{3.10}$$

which can be simplified for the symmetric Duffing potential ($\alpha = 0$) to obtain [2, 19]

$$I_0^{l,r} = \pi\omega\sqrt{\frac{2}{\beta}}\operatorname{sech}\frac{\omega\pi}{2\sqrt{-\eta}}. \tag{3.11}$$

For the integral $I_1^{l,r}$ and $I_j^{l,r}$ one obtains

$$\begin{aligned} I_1^{l,r} &= \int_{-\infty}^{+\infty} x_0^{l,r} y_0^{l,r} \sin\omega t\, dt = \mathbf{K_1}(1,1,\omega) \\ &= \frac{(\eta-\omega^2)\omega\pi}{3\Delta\sinh(\omega\pi/\sqrt{-\eta})}\,{}_2\mathbf{F_1}\left(1 - J\frac{\omega}{2\sqrt{-\eta}}, 1 + J\frac{\omega}{2\sqrt{-\eta}}; \frac{5}{2}; \xi\right), \end{aligned} \tag{3.12}$$

which takes the expression corresponding to the parametrically driven Duffing equation [8]

$$I_1^{l,r} = -\frac{\pi\omega^2}{\beta}\operatorname{sech}\frac{\omega\pi}{2\sqrt{-\eta}}. \tag{3.13}$$

For the integrals $I_2^{l,r}$, we obtain, respectively

$$\begin{aligned} I_2^{l,r} &= \int_{-\infty}^{+\infty} x_0^{l,r2} y_0^{l,r} \sin\omega t\, dt = \mathbf{K_1}(2,1,\omega) \\ &= \frac{\pm\pi\omega^2(\eta-\omega^2)(4\eta-\omega^2)}{90\Delta^{\frac{3}{2}}\sinh(\omega\pi/\sqrt{-\eta})}\,{}_2\mathbf{F_1}\left(\frac{3}{2} - J\frac{\omega}{2\sqrt{-\eta}}, \frac{3}{2} + J\frac{\omega}{2\sqrt{-\eta}}; \frac{7}{2}; \xi\right), \\ I_3^{l,r} &= \int_{-\infty}^{+\infty} x_0^{l,r3} y_0^{l,r} \sin\omega t\, dt = \mathbf{K_1}(3,1,\omega) \\ &= \frac{\pi\omega^2(\eta-\omega^2)(4\eta-\omega^2)(9\eta-\omega^2)}{7560\Delta^{3/2}\sinh(\omega\pi/\sqrt{-\eta})}\,{}_2\mathbf{F_1}\left(2 - J\frac{\omega}{2\sqrt{-\eta}}, 2 + J\frac{\omega}{2\sqrt{-\eta}}; \frac{7}{2}; \xi\right). \end{aligned} \tag{3.14}$$

Finally, the integral $I_i^{l,r}$, $i \in (4,5,6,7)$ are given by

$$I_i^{l,r} = \int_{-\infty}^{+\infty} x_0^{l,ri} y_0^{l,r} \cos\omega t\, dt = \mathbf{K_2}(i,1,\omega) = 0. \tag{3.15}$$

Using the Melnikov criterion [13], one concludes that nonperiodic motions appear when

$$r > r_c = \frac{1}{\omega^2}\left|\frac{\lambda J_0^{l,r}}{\left[\sum_{i=0}^{i=3}\zeta_i I_i\right]}\right|. \tag{3.16}$$

This criterion defines the threshold value for the appearance of transverse intersection between the perturbed and unperturbed manifolds. This threshold condition is plotted in Figure 3 as a function of the excitation frequency ω for different values of the incline γ and as a function of γ for $\omega = 1.5$ with $\lambda = 0.2$, $\eta = -1$, $\alpha = 0.075$, $\beta = 0.5$, and for the plus sign in (3.2).

Figure 3(a) shows a classical result, that is, in the chosen interval $\omega \in [0, 8]$, the threshold value of r decreases for small values of the frequency and increases for large values of the frequency. A singularity is obtained for $\gamma = \pi/2$ (red lines) indicating that the bifurcation curve splits into two lobes creating a domain of a regular motion near a certain value of the frequency ω. Figure 3(b) illustrates the effect of the tilted angle of the excitation γ on the bifurcation curves for $\omega = 1.5$. It appears from this figure that the threshold r_c increases with γ until a critical value and then decreases. The domain of periodic motion is larger near the vertical excitation ($\gamma \approx \pi/2$) than near the horizontal one ($\gamma = 0$).

To test the validity of the Melnikov predictions, we investigate the regular or irregular (fractal) shape of the basins of attraction [14]. A basin with smooth shape will suggest regular dynamics of the system while a fractal basin will indicate nonregular dynamic. The basins are plotted using a simplified criterion which distinguish solutions of mean value displacement. This is done by scanning the initial values x_0 and y_0 of x and y in $[-3.5, 3.5] \times [-3.5, 3.5]$ domain, solving numerically (2.3) and collecting the initial conditions which attract the dynamics in the right (for instance) well of the potential (marked region of the basin). The unmarked region represents the domain for which the system dynamics is attracted to the other well. In a more detailed approach, a larger number of basins would illustrate other signatures of the system response hidden in the figure. The effect of γ on the shape of the basins of attraction of Figure 4 are plotted for the values of Figure 3(a). The graph of Figure 4(a) is plotted for $r = 0.05$, $\omega = 1.5$, and $\gamma = \pi/2$ showing a regular behavior of the system which is consistent with the Melnikov prediction. Figure 4(b) shows how the shape of the basin becomes fractal for $r = 0.1 > r_c$. The fractal shape is more pronounced as r increases as illustrated in Figure 4(c) ($r = 0.15$) and Figure 4(d) ($r = 0.2$). Choosing r close to the critical value r_c may not lead to the same conclusion as illustrated in Figure 4(b) since the Melnikov function is a first-order approximation [14]. These results show that the final state of the system highly depends upon initial conditions and the tilt angle is the key parameter. This strong dependency of the system upon initial conditions was obtained experimentally by Mann [21] for a perfectly horizontal excitation based on energy criterion analysis.

4. Effect of Parametric Damping

The idea of controlling a pendulum via feedback parametric damping was recently investigated experimentally by Kraftmakher [31]. In his experiment, the voltage was collected through a coil, amplified and reinjected in the system for the purpose of control. In such a process the system may experience fluctuations arising as noise, lost signal, and additional resonant excitation. These fluctuations can be modeled as a harmonic function of time. In such a situation, (2.3) under parametric damping can be written as

$$\frac{d^2x}{dt^2} + [\lambda \pm \Gamma_1 x + \Gamma_2 \sin \tilde{\omega} t]\frac{dx}{dt} + \eta x + \alpha x^2 + \beta x^3 = f(t), \tag{4.1}$$

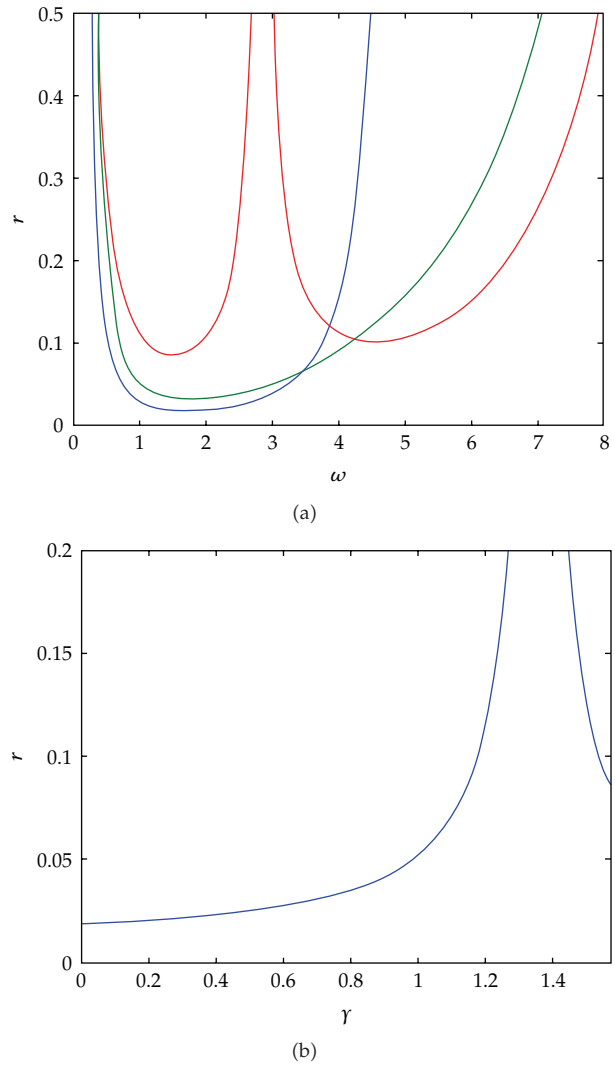

Figure 3: Critical amplitude r for the appearance of nonperiodic motion as function of the system parameters for $\lambda = 0.2$, $\eta = -1$, $\alpha = 0.075$, and $\beta = 0.5$. The domain under a line is where a periodic motion is guaranteed. Blue line $\gamma = 0$, red line $\gamma = \pi/2$, and green line $\gamma = \pi/4$. (a) r as function of the driving frequency ω; (b) r as function of the tilt angle γ for $\omega = 1.5$.

where Γ_1 and Γ_2 are the feedback gains of parametric damping. The plus sign is taken for negative feedback and the minus is for positive feedback [26]. By applying the Melnikov theorem, one obtains

$$M(t_0) = \int_{-\infty}^{+\infty} \mathbf{F}(x, y) \times \mathbf{G}^*(x, y, t - t_0)\, dt, \tag{4.2}$$

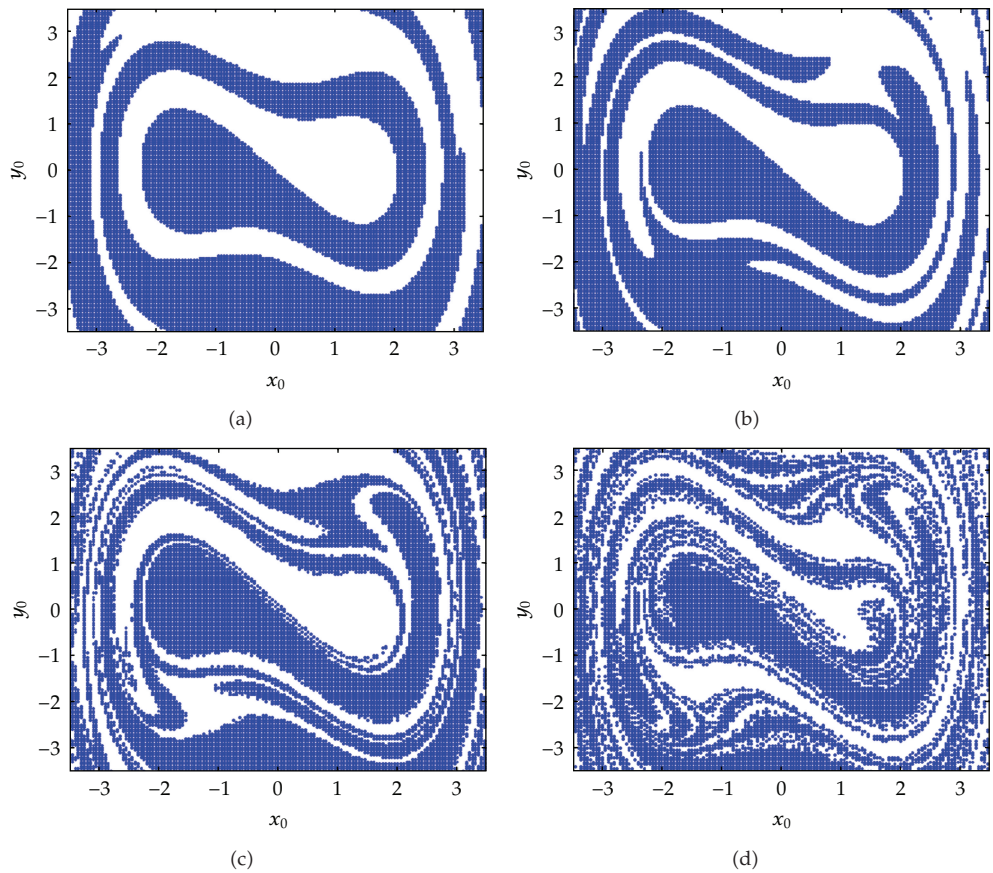

Figure 4: Evolution of the shape of the basin of attraction of the right well as r increases for $\omega = 1.5$, $\gamma = \pi/2$, and the value of Figure 2. (a) $r = 0.05$, (b) $r = 0.1$, (c) $r = 0.15$, and (d) $r = 0.2$. The basins have been obtained using a simplified criterion which distinguish solution of mean value of displacement. The marked region corresponds to the region for which the dynamics is attracted in the right well.

with

$$\mathbf{G}^*(x, y, t - t_0) = \begin{pmatrix} 0 \\ -\left[\lambda^* \pm \Gamma_1^* x + \Gamma_2^* \sin \tilde{\omega}(t - t_0)\right] y + r^* \omega^2 \left[\sum_{i=0}^{i=3} \zeta_i x^i\right] \cos \omega(t - t_0) \end{pmatrix}, \tag{4.3}$$

$\Gamma_1 = \epsilon \Gamma_1^*$ and $\Gamma_2 = \epsilon \Gamma_2^*$.

From (4.2), the Melnikov function reads

$$\begin{aligned} M(t_0) = &-\left[\lambda J_0^{l,r} \pm \Gamma_1 J_2^{l,r} + \Gamma_2 J_2^{l,r} \sin \tilde{\omega} t_0 + \Gamma_2 J_3^{l,r} \cos \tilde{\omega} t_0\right] \\ &+ r\omega^2 \left[\sum_{i=0}^{i=3} \zeta_i I_i\right] \sin \omega t_0 + r\omega^2 \left[\sum_{i=0}^{i=3} \zeta_i I_{i+4}\right] \cos \omega t_0, \end{aligned} \tag{4.4}$$

in which

$$J_1^{l,r} = \int_{-\infty}^{+\infty} x_0^{l,r} y_0^{l,r}\, dt = \pm \frac{\eta^3\sqrt{-\eta}}{105\Delta^{3/2}}\, {}_2\mathbf{F}_1\left(\frac{3}{2}, \frac{5}{2}; \frac{9}{2}; \xi\right),$$
$$J_2^{l,r} = \int_{-\infty}^{+\infty} y_0^{l,r2} \cos\tilde{\omega} t\, dt = -\frac{81\eta^3\Delta}{4\alpha^2\sqrt{-\eta}} \int_{-1}^{+1} \frac{\sinh^2 u \cos au}{(1-v^2)[1+\kappa\cosh u]}\, dv, \tag{4.5}$$

with $\kappa = \pm(3\sqrt{\Delta}/2\alpha)$, $u = \tanh^{-1} v$, $a = \tilde{\omega}/\sqrt{-\eta}$, and

$$J_3^{l,r} = \int_{-\infty}^{+\infty} y_0^{l,r2} \sin\tilde{\omega} t\, dt = 0, \tag{4.6}$$

as a product of even and odd function. Thus the Melnikov function becomes

$$M(t_0) = -\left[\lambda J_0^{l,r} \pm \Gamma_1 J_2^{l,r} + \Gamma_2 J_2^{l,r} \sin\tilde{\omega} t_0\right] + r\omega^2 \left[\sum_{i=0}^{i=3} \zeta_i I_i\right] \sin\omega t_0. \tag{4.7}$$

In the absence of the periodic feedback fluctuation ($\Gamma_2 = 0$), the threshold condition for the appearance of chaos of the asymmetric pendulum with parametric damping and tilted excitation is given by

$$r > r_c = \frac{1}{\omega^2} \left| \frac{\lambda J_0^{l,r} \pm \Gamma_1 J_1^{l,r}}{\left[\sum_{i=0}^{i=3} \zeta_i I_i\right]} \right|. \tag{4.8}$$

Figure 5 illustrates the effect of the parametric damping component (Γ_1) on the threshold of Figure 3 in the absence of the harmonic fluctuation ($\Gamma_2 = 0$). In this figure, the red line is plotted for a positive feedback ($\Gamma_1 = -0.5$), the green line is for a negative feedback ($\Gamma_1 = 0.5$), and the blue line corresponds to the case without feedback gain ($\Gamma_1 = 0$). The graphs show that the negative feedback is effictive for enhancement of chaos by increasing the bound value delimiting chaotic domain, while the positive feedback is effictive in suppressing chaos by decreasing the threshold curve for chaos. A rapid analysis of (4.8) shows clearly that r_c increases with Γ_1 (negative feedback) and linearly decreases with Γ_1 (positive feedback).

In the presence of the periodic fluctuation in the parametric damping ($\Gamma_2 \neq 0$), one obtains from (4.7) the following under resonance conditions

$$\lambda J_0^{l,r} \pm \Gamma_1 J_2^{l,r} = \left[\Gamma_2 J_2^{l,r} + r\omega^2 \left[\sum_{i=0}^{i=3} \zeta_i I_i\right]\right] \sin\tilde{\omega} t_0. \tag{4.9}$$

Hence, the periodic motion is guaranteed if

$$\left| \frac{\lambda J_0^{l,r} \pm \Gamma_1 J_2^{l,r}}{\Gamma_2 J_2^{l,r} + r\omega^2 \left[\sum_{i=0}^{i=3} \zeta_i I_i\right]} \right| < 1. \tag{4.10}$$

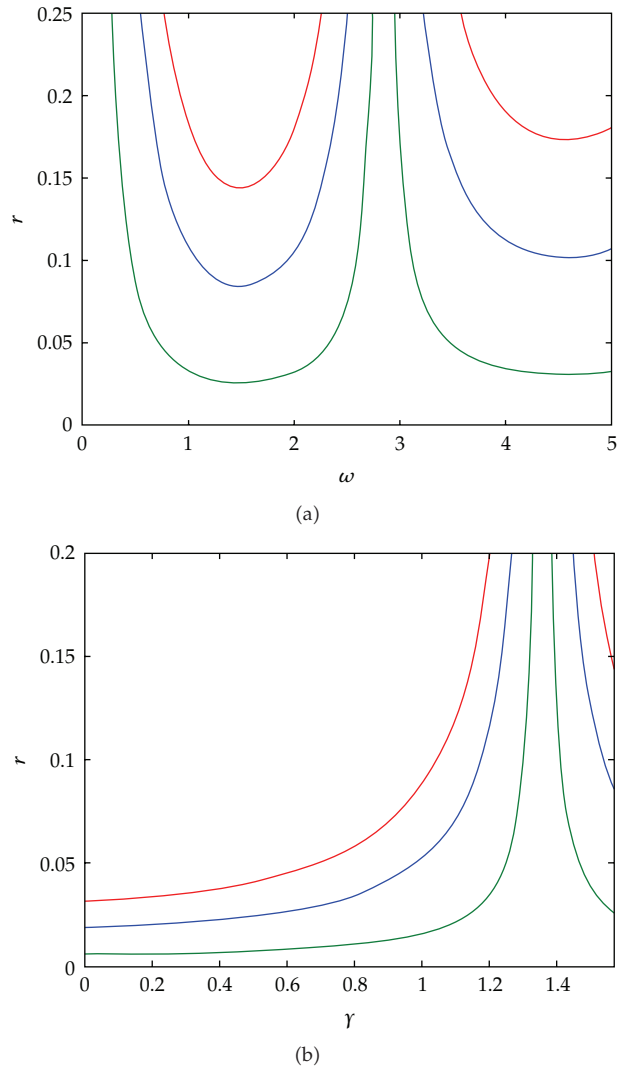

Figure 5: Effect of the parametric damping on the threshold condition for chaos with $\Gamma_2 = 0$ and the values of Figure 2. (a) Effect with $\gamma = \pi/2$ in (r, ω) plane. (b) Effect with $\omega = 1.5$ in (r, γ) plane. The green line corresponds to the negative feedback ($\Gamma_1 = 0.5$). The red line corresponds to the positive feedback ($\Gamma_1 = -0.5$). The blue line corresponds to the case without control ($\Gamma_1 = 0$).

Figure 5 shows the effect of the feedback gain Γ_1 on the domain of chaotic dynamics for $r = 0.2$ and $\gamma = \pi/2$. It can be seen from the plots that by decreasing the feedback gain from $\Gamma_1 = 0$ (Figure 6(a)) to $\Gamma_1 = -0.75$ (Figure 6(c)), the area of regular motions (marked domain) increases.

Figure 7 illustrates the influence of the incline of the excitation γ on the chaotic domain for the given value $\Gamma_1 = -0.5$. The plots in this figure indicate that as γ increases from horizontal ($\gamma = 0$, Figure 7(a)) to vertical ($\gamma = \pi/2$, Figure 7(c)), the area of regular motions decreases with a singularity at $\gamma = \pi/2$ as shown in Figures 3(b) and 7(c).

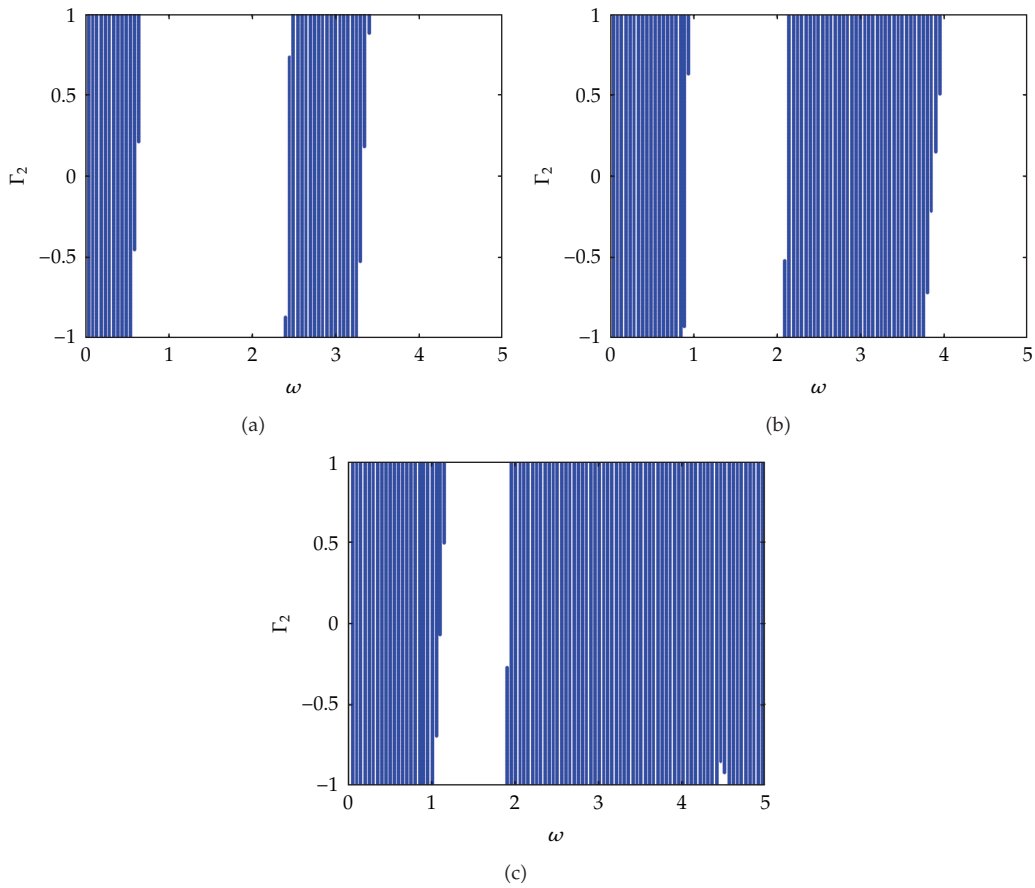

Figure 6: Effect of sinusoidal fluctuation on the control strategy for $r = 0.2$, $\gamma = \pi/2$, and the values of Figure 4(a) in (ω, Γ_2) plan. (a) $\Gamma_1 = 0$, (b) $\Gamma_1 = -0.5$, and (c) $\Gamma_1 = -0.75$. The marked domain corresponds to the area of regular motion.

5. Conclusion

The effect of a tilted parametric excitation and of parametric damping with periodic fluctuation on the appearance of chaos in an asymmetric magnetic pendulum was examined. The analysis was carried out using the Melnikov method to derive the analytical condition for chaotic motions. These analytical predictions were tested and validated by exploring the fractal and regular shapes of the basins of attraction. It was shown that in the absence of the parametric damping components ($\Gamma_1 = 0$, $\Gamma_2 = 0$), the incline angle of the excitation can influence the chaotic dynamic of the magnetic pendulum. In other words, as the tilt angle of the excitation increases from horizontal ($\gamma = 0$) to the vertical ($\gamma = \pi/2$) position, the domain of regular motion increases (Figure 2). This suggests that stability can be gained when the tilting excitation approaches the vertical position, which is consistent with the results given in [32].

Furthermore, in the presence of the incline of the excitation and of the parametric damping without periodic fluctuation ($\Gamma_1 \neq 0$, $\Gamma_2 = 0$), the results show that a positive feedback gain ($\Gamma_1 = -0.5$) enlarges the domain of periodicity while a negative feedback gain ($\Gamma_1 = 0.5$) extends the region of chaotic regime (Figure 5). On the other hand, in the case

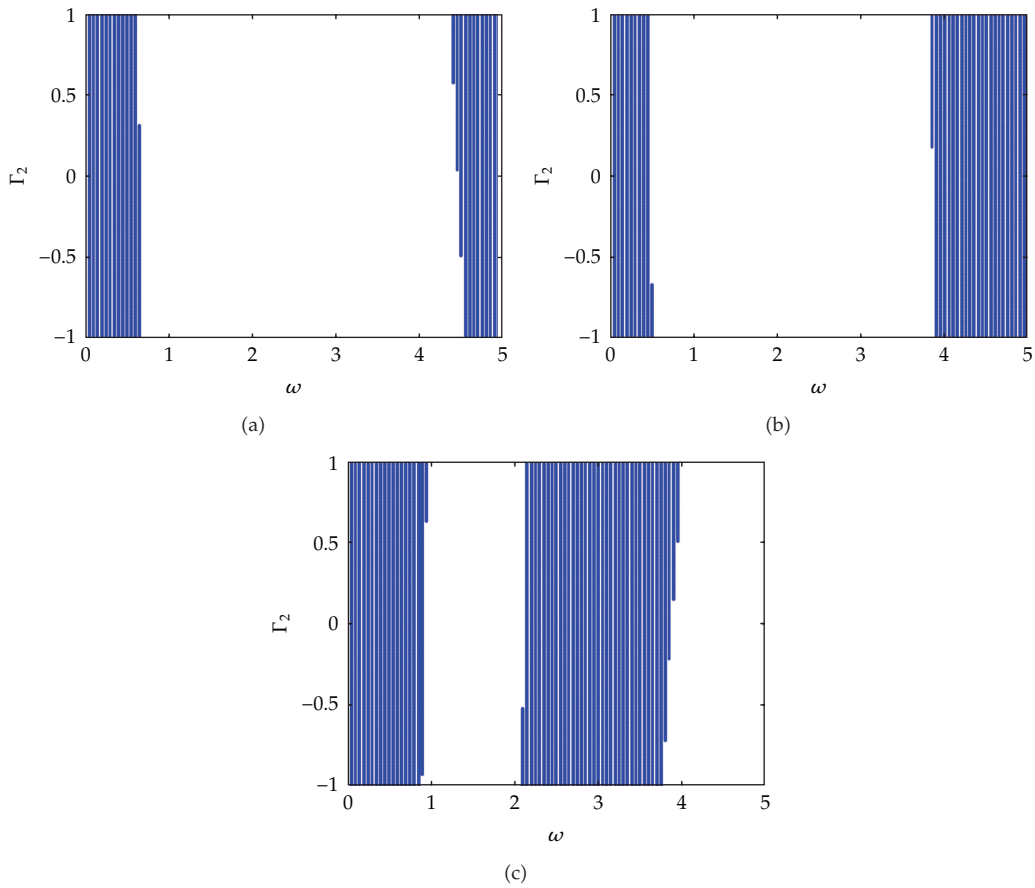

Figure 7: Effect of sinusoidal fluctuation on the control strategy for $r = 0.2$, $\Gamma_1 = -0.5$, and the values of Figure 4(a) in (ω, Γ_2) plan. (a) $\gamma = 0$, (b) $\gamma = \pi/4$, and (c) $\gamma = \pi/2$. The marked domain corresponds to the area of regular motion.

where the parametric damping with harmonic fluctuation is introduced, the area of regular motions increases with decreasing the feedback gain Γ_1 (Figure 6) and this area increases by increasing the incline from a horizontal to a vertical direction, as expected (Figure 7).

The results of this work show that chaotic dynamics can be controlled in an asymmetric magnetic pendulum by acting either on the incline of parametric excitation or on feedback gains of a parametric damping, or on both. This provides some interesting possibilities for controlling the dynamics in asymmetric magnetic pendulums.

Appendices

A. Functional Relation of the Gamma Function Γ

Consider the following:

$$\Gamma(z+1) = z\Gamma(z),$$

$$\Gamma(1+Ja)\Gamma(1-Ja) = \frac{\pi a}{\sinh \pi a},$$

$$\Gamma\left(\frac{1+Ja}{2}\right)\Gamma\left(\frac{1-Ja}{2}\right) = \frac{\pi}{\cosh \pi a},$$
$$\Gamma\left(n+\frac{1}{2}\right) = (2n-1)!\frac{\sqrt{n}}{2^n},$$
$$\Gamma(n) = (n-1)!. \tag{A.1}$$

B. Functional Relation between the Associated Lengendre Function of the Second Kind and the Gauss Hypergeometric Function

Consider

$$\mathbf{Q}_{\mu}^{\nu}(z) = \frac{e^{J\nu\pi}\Gamma(\nu+\mu+1)\Gamma(1/2)}{2^{1+\mu}\Gamma(\mu+3/2)}\left(z^2-1\right)^{\nu/2} z^{-\mu-\nu-1}\,{}_2\mathbf{F}_1\left(\frac{\mu+\nu+2}{2}, \frac{\mu+\nu+1}{2}; \mu+\frac{3}{2}; \frac{1}{\xi}\right). \tag{B.1}$$

C. Properties of the Gauss Hypergeometric Function

Consider

$${}_2\mathbf{F}_1(a,b,c,z) = \sum_{n=0}^{+\infty} \frac{(a)_n (b)_n}{(c)_n} \frac{z^n}{n!}, \quad |z| < 1, \tag{C.1}$$

and the Pochhammer symbol is defined as

$$(a)_n = a(a+1)(a+2)\cdots(a+n-1), \qquad (a)_0 = 1, \tag{C.2}$$

then, if $a = \overline{b}$, one has

$${}_2\mathbf{F}_1(a,\overline{a},c,z) = \sum_{n=0}^{+\infty} \frac{(a)_n (\overline{a})_n}{(c)_n} \frac{z^n}{n!}, \quad |z| < 1, \tag{C.3}$$

this last expression of ${}_2\mathbf{F}_1(a,\overline{a},c,z)$ is always a positive real number.

Acknowledgements

This work is supported by the US Office of Naval Research under the Grant ONR N00014-08-1-0435. Thanks are due to Mr. Anthony Seman III of ONR and Dr. Stephen Mastro of NAVSEA, Philadelphia PA, USA.

References

[1] S. K. De and N. R. Aluru, "Complex oscillations and chaos in electrostatic microelectromechanical systems under superharmonic excitations," *Physical Review Letters*, vol. 94, no. 20, 4 pages, 2005.

[2] B. E. DeMartini, H. E. Butterfield, J. Moehlis, and K. L. Turner, "Chaos for a microelectromechanical oscillator governed by the nonlinear mathieu equation," *Journal of Microelectromechanical Systems*, vol. 16, no. 6, pp. 1314–1323, 2007.

[3] H. M. Ouakad and M. I. Younis, "The dynamic behavior of MEMS arch resonators actuated electrically," *International Journal of Non-Linear Mechanics*, vol. 45, no. 7, pp. 704–713, 2010.

[4] I. Eker, "Experimental on-line identification of an electromechanical system," *ISA Transactions*, vol. 43, no. 1, pp. 13–22, 2004.

[5] C. A. K. Kwuimy and P. Woafo, "Dynamics, chaos and synchronization of self-sustained electromechanical systems with clamped-free flexible arm," *Nonlinear Dynamics*, vol. 53, no. 3, pp. 201–213, 2008.

[6] C. A. Kitio Kwuimy, B. Nana, and P. Woafo, "Experimental bifurcations and chaos in a modified self-sustained macro electromechanical system," *Journal of Sound and Vibration*, vol. 329, no. 15, pp. 3137–3148, 2010.

[7] A. H. Nayfeh and D. T. Mook, *Nonlinear Oscillations*, Wiley-Interscience, New York, NY, USA, 1979.

[8] B. R. Nana Nbendjo and P. Woafo, "Active control with delay of horseshoes chaos using piezoelectric absorber on a buckled beam under parametric excitation," *Chaos, Solitons & Fractals*, vol. 32, no. 1, pp. 73–79, 2007.

[9] A. O. Belyakov, A. P. Seyranian, and A. Luongo, "Dynamics of the pendulum with periodically varying length," *Physica D*, vol. 238, no. 16, pp. 1589–1597, 2009.

[10] G. Litak, M. Wiercigroch, B. W. Horton, and X. Xu, "Transient chaotic behaviour versus periodic motion of a parametric pendulum by recurrence plots," *ZAMM Zeitschrift für Angewandte Mathematik und Mechanik*, vol. 90, no. 1, pp. 33–41, 2010.

[11] C. Hayashi, *Nonlinear Oscillations in Physical Systems*, McGraw-Hill Electrical and Electronic Engineering Series, McGraw-Hill, New York, NY, USA, 1964.

[12] A. Oksasoglu and D. Vavriv, "Interaction of low- and high-frequency oscillations in a nonlinear RLC circuit," *IEEE Transactions on Circuits and Systems I*, vol. 41, no. 10, pp. 669–672, 1994.

[13] B. Nana and P. Woafo, "Synchronization in a ring of four mutually coupled van der Pol oscillators: theory and experiment," *Physical Review E*, vol. 74, no. 4, Article ID 046213, 8 pages, 2006.

[14] S. Wiggins, *Introduction to Applied Nonlinear Dynamical Systems and Chaos*, vol. 2 of *Texts in Applied Mathematics*, Springer, New York, NY, USA, 1990.

[15] O. Diallo and Y. Koné, "Melnikov analysis of chaos in a general epidemiological model," *Nonlinear Analysis: Real World Applications*, vol. 8, no. 1, pp. 20–26, 2007.

[16] Z. Zhang, J. Peng, and J. Zhang, "Melnikov method to a bacteria-immunity model with bacterial quorum sensing mechanism," *Chaos, Solitons & Fractals*, vol. 40, no. 1, pp. 414–420, 2009.

[17] G. Cicogna and F. Papoff, "Asymmetric duffing equation and the appearance of chaos," *Europhysics Letters*, vol. 3, no. 9, pp. 963–967, 1978.

[18] S. Lenci and G. Rega, "Global optimal control and system-dependent solutions in the hardening Helmholtz-Duffing oscillator," *Chaos, Solitons & Fractals*, vol. 21, no. 5, pp. 1031–1046, 2004.

[19] G. Litak, A. Syta, and M. Borowiec, "Suppression of chaos by weak resonant excitations in a non-linear oscillator with a non-symmetric potential," *Chaos, Solitons & Fractals*, vol. 32, no. 2, pp. 694–701, 2007.

[20] H. Cao, J. M. Seoane, and M. A. F. Sanjuán, "Symmetry-breaking analysis for the general Helmholtz-Duffing oscillator," *Chaos, Solitons & Fractals*, vol. 34, no. 2, pp. 197–212, 2007.

[21] B. P. Mann, "Energy criterion for potential well escapes in a bistable magnetic pendulum," *Journal of Sound and Vibration*, vol. 323, no. 3–5, pp. 864–876, 2009.

[22] J. J. Thomsen, "Effective properties of mechanical systems under high-frequency excitation at multiple frequencies," *Journal of Sound and Vibration*, vol. 311, no. 3–5, pp. 1249–1270, 2008.

[23] M. V. Bartuccelli, G. Gentile, and K. V. Georgiou, "On the dynamics of a vertically driven damped planar pendulum," *The Royal Society of London. Proceedings. Series A*, vol. 457, no. 2016, pp. 3007–3022, 2001.

[24] J. M. Schmitt and P. V. Bayly, "Bifurcations in the mean angle of a horizontally shaken pendulum: analysis and experiment," *Nonlinear Dynamics*, vol. 15, no. 1, pp. 1–14, 1998.

[25] H. Yabuno, M. Miura, and N. Aoshima, "Bifurcation in an inverted pendulum with tilted high-frequency excitation: analytical and experimental investigations on the symmetry-breaking of the bifurcation," *Journal of Sound and Vibration*, vol. 273, no. 3, pp. 493–513, 2004.

[26] B. P. Mann and M. A. Koplow, "Symmetry breaking bifurcations of a parametrically excited pendulum," *Nonlinear Dynamics*, vol. 46, no. 4, pp. 427–437, 2006.

[27] M. Belhaq and S. Mohamed Sah, "Fast parametrically excited van der Pol oscillator with time delay state feedback," *International Journal of Non-Linear Mechanics*, vol. 43, no. 2, pp. 124–130, 2008.

[28] S. Sah and M. Belhaq, "Effect of vertical high-frequency parametric excitation on self-excited motion in a delayed van der Pol oscillator," *Chaos, Solitons & Fractals*, vol. 37, no. 5, pp. 1489–1496, 2008.

[29] A. Fidlin and J. Juel Thomsen, "Non-trivial effects of high-frequency excitation for strongly damped mechanical systems," *International Journal of Non-Linear Mechanics*, vol. 43, no. 7, pp. 569–578, 2008.

[30] F. C. Moon, J. Cusumano, and P. J. Holmes, "Evidence for homoclinic orbits as a precursor to chaos in a magnetic pendulum," *Physica D*, vol. 24, no. 1–3, pp. 383–390, 1987.

[31] Y. Kraftmakher, "Experiments with a magnetically controlled pendulum," *European Journal of Physics*, vol. 28, no. 5, pp. 1007–1020, 2007.

[32] S. M. Sah and M. Belhaq, "Control of a delayed limit cycle using the tilt angle of a fast excitation," *Journal of Vibration and Control*, vol. 17, no. 2, pp. 175–182, 2011.

[33] I. S. Gradstein and I. M. Rjikhik, *Table of Integrals, Series and Products*, Nauka, Moscow, Russia, 1971.

[34] http://www.gnu.org/software/gsl/manual/html_node/.

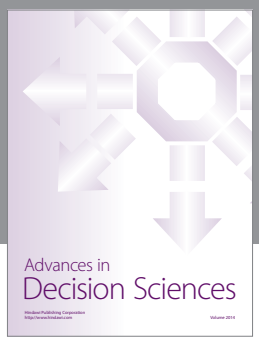

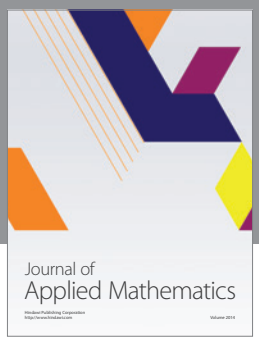

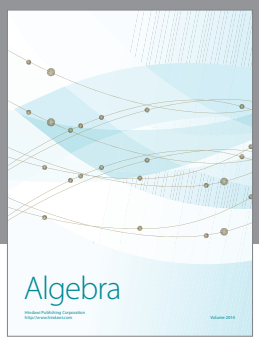

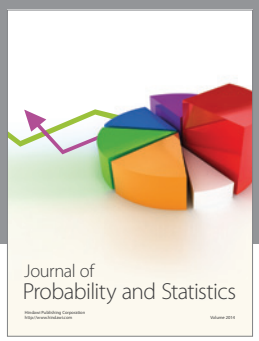

Hindawi
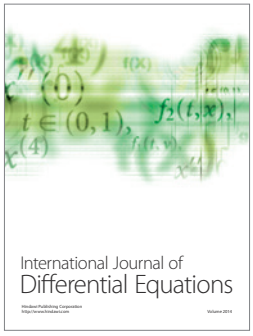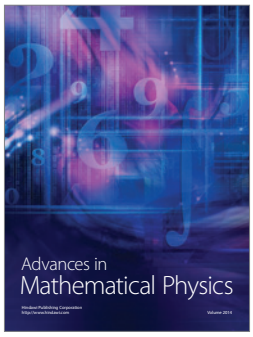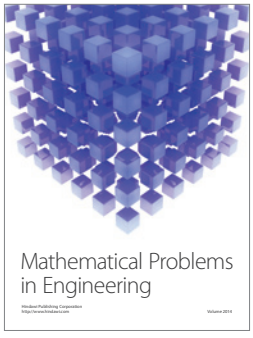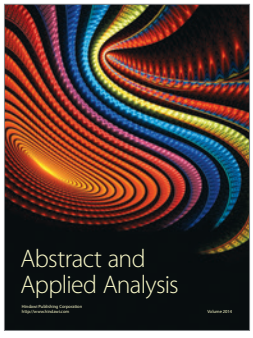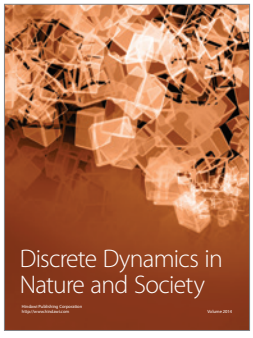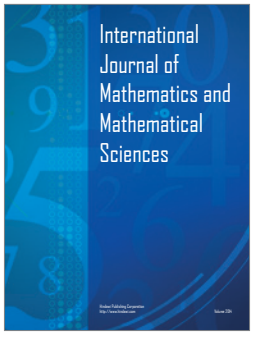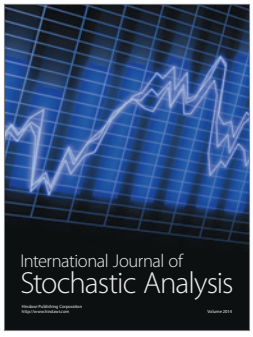
Submit your manuscripts at
http://www.hindawi.com